RESEARCH ARTICLE

Figures and figure supplements

Pore mutation N617D in the skeletal muscle DHPR blocks Ca^{2+} influx due to atypical high-affinity Ca^{2+} binding

Anamika Dayal *et al*

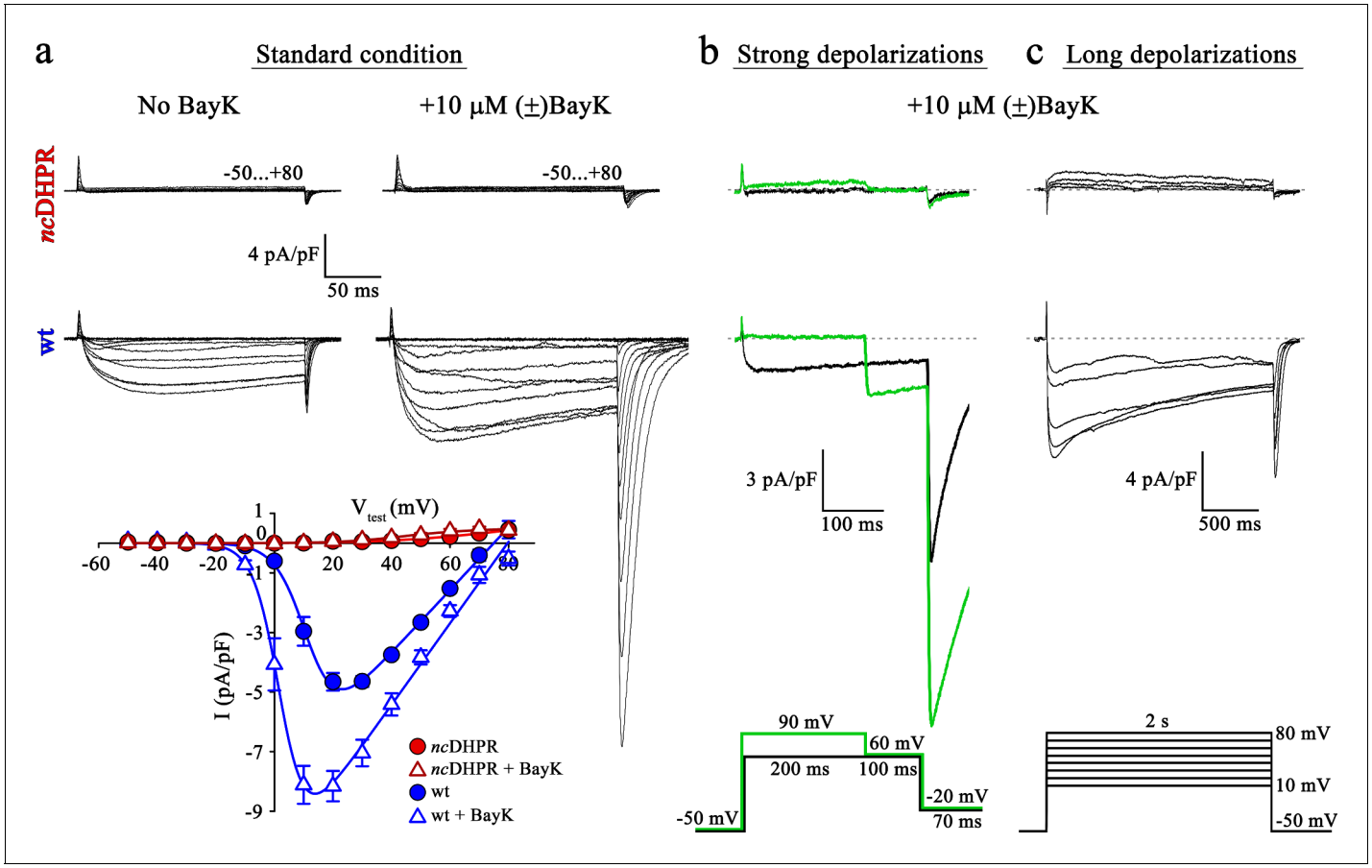

Figure 1. Mutant DHPR(N617D) remains Ca^{2+} impermeant despite strong or long depolarizations in the presence of DHP agonist Bay K. (**a**) Representative whole-cell Ca^{2+} current recordings elicited by 200 ms depolarizations from −50 to +80 mV from *nc*DHPR (*top*) and wt (*center*) myotubes before (*left*) and after (*right*) perfusion with 10 µM of the DHP agonist (±)Bay K 8644. Scale bars, 50 ms (horizontal), 4 pA/pF (vertical). Plots of current-voltage relationship (*bottom*) indicates lack of DHPR inward Ca^{2+} currents in the absence (I_{max} = −0.02 ± 0.01 pA/pF; *n* = 8) and presence (I_{max} = −0.02 ± 0.01 pA/pF; *n* = 5) of (±)Bay K through *nc*DHPR myotubes, in contrast to significant (p<0.001) augmentation of Ca^{2+} currents in wt myotubes upon administration of (±)Bay K (No Bay K: I_{max} = −5.04 ± 0.27 pA/pF; *n* = 9; with Bay K: I_{max} = −8.82 ± 0.56 pA/pF; *n* = 6). (**b**) 200 ms strong depolarization to +90 mV followed by 100 ms to +60 mV and finally repolarization to −20 mV for 70 ms (*bottom, green lines*) in the presence of 10 µM (±)Bay K, were unable to evoke inward Ca^{2+} currents through DHPR(N617D) (*top*, with +90 mV prepulse: I_{max} = −0.02 ± 0.02 pA/pF; without +90 mV prepulse: I_{max} = 0.01 ± 0.02 pA/pF; *n* = 10). Contrary, wt DHPR displayed significant (p<0.01) depolarization-induced potentiation of inward current at +60 mV (with +90 mV prepulse: I_{max} = −2.97 ± 0.54 pA/pF; without +90 mV prepulse: I_{max} = −1.62 ± 0.37 pA/pF; *n* = 5) (*center*). Upon subsequent repolarization from +60 mV to −20 mV, the tail current was also considerably larger (p<0.01) after the +90 mV pre-conditioning pulse (I_{tail} = −19.36 ± 3.59 pA/pF; *n* = 5) (*center, green trace*) than after the +60 mV pulse (I_{tail} = −10.78 ± 1.99 pA/pF; *n* = 5) (*center, black trace*). Statistical significance was calculated using paired *t*-test. Scale bars, 100 ms (horizontal), 3 pA/pF (vertical). (**c**) Likewise, 2 s long depolarizations from +10 mV to +80 mV in 10 mV increments (*bottom*) in the presence of 10 µM (±)Bay K, were unable to induce Ca^{2+} influx through DHPR(N617D) (*top*, I_{max} = −0.05 ± 0.02 pA/pF; *n* = 5). The same voltage protocol evoked robust inward Ca^{2+} currents through wt DHPR (*center*, I_{max} = −7.69 ± 0.56 pA/pF; *n* = 5). Scale bars, 500 ms (horizontal), 4 pA/pF (vertical). Data are presented as mean ± SEM; p determined by unpaired Student's *t*-test.

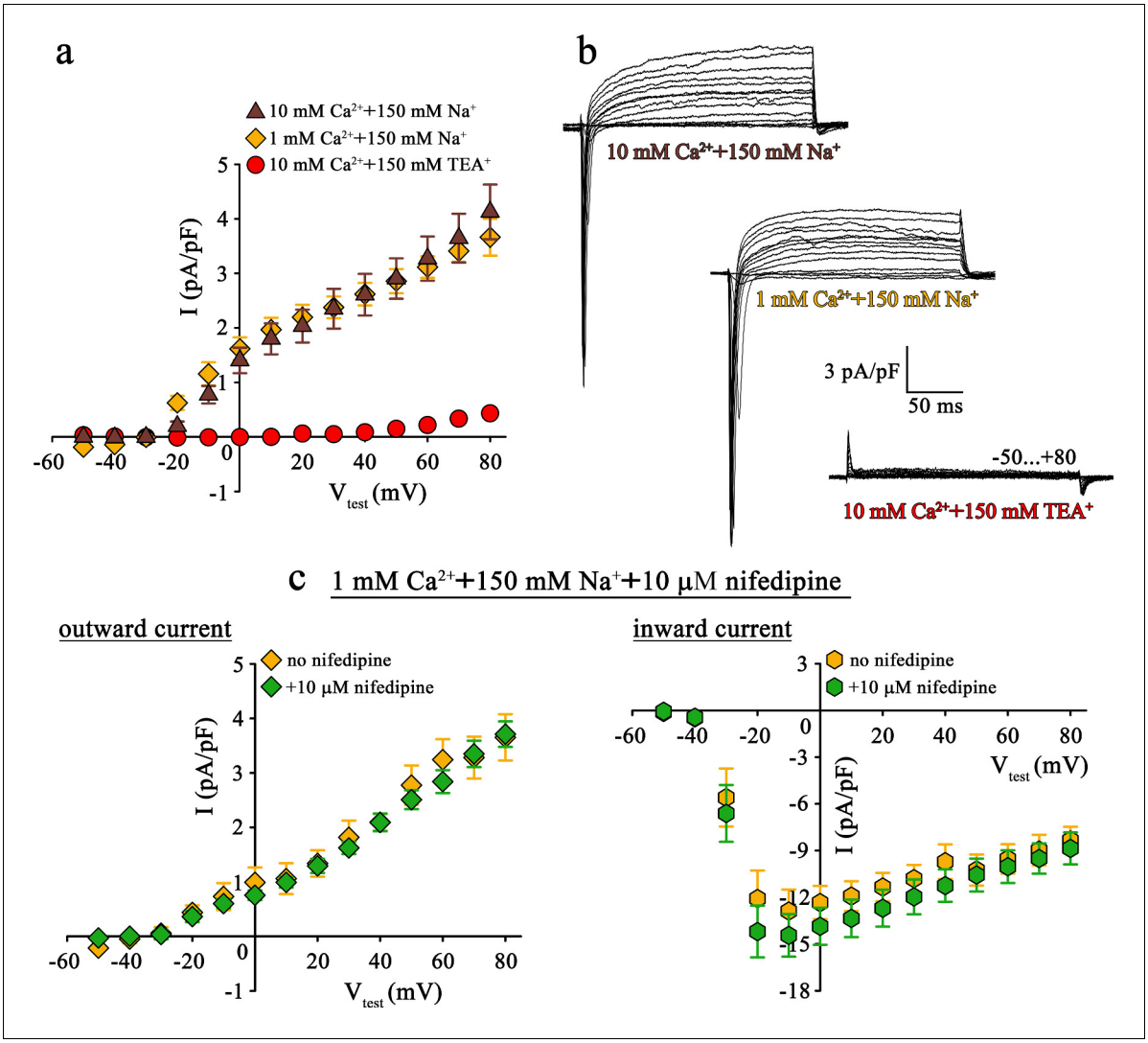

Figure 2. Mutant DHPR(N617D) does not conduct inward Na^+ currents in the presence of near physiological [Na^+]. (**a**) Plots of current-voltage relationship for DHPR-mediated Na^+ currents recorded from *nc*DHPR myotubes indicate the absence of slow-activating, non-inactivating inward Na^+ currents in the presence of near physiological 150 mM external Na^+ with either 10 mM (n = 8) or 1 mM external Ca^{2+} (n = 9). Control recordings were performed in standard bath solution (150 mM TEA^+, 10 mM Ca^{2+}) (n = 8). (**b**) Representative current recordings from *nc*DHPR myotubes in response to 200 ms depolarizing test pulses between −50 to +80 mV in the presence of 10 mM Ca^{2+} with either 150 mM Na^+ (*top*) or 150 mM TEA^+ (*bottom*), or 1 mM Ca^{2+} with 150 mM Na^+ (*center*) in the bath solution. Scale bars, 50 ms (horizontal), 3 pA/pF (vertical). (**c**) Plots of current-voltage relationship for *nc*DHPR myotubes at 150 mM external Na^+ and 1 mM external Ca^{2+} indicate no difference ($p>0.05$) in outward and inward currents in the presence (n = 10) and absence (n = 6) of 10 µM of the 1,4-DHP antagonist nifedipine.

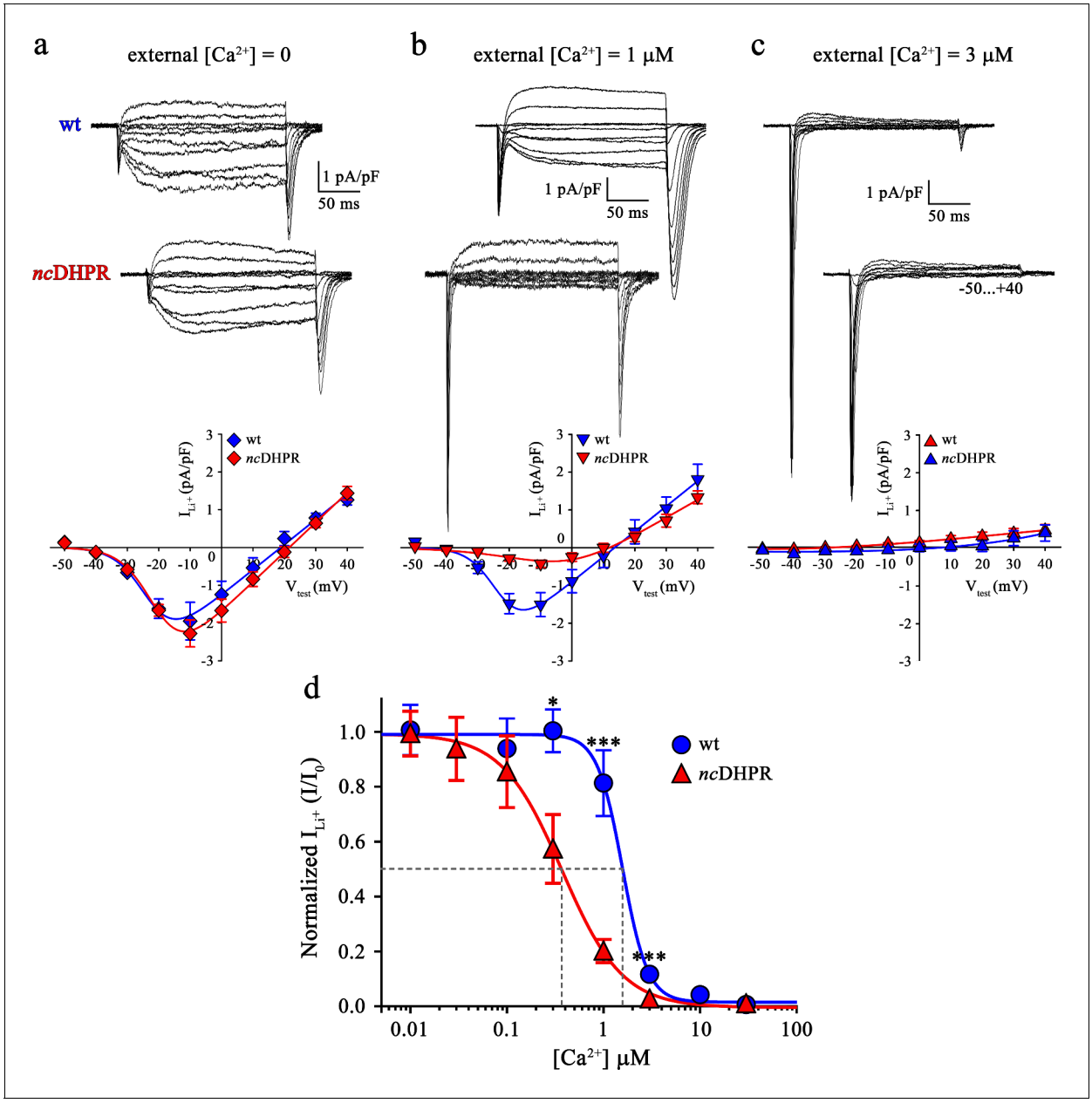

Figure 3. Binding of Ca^{2+} ions with nanomolar affinity within the pore of mutant DHPR(N617D) precludes Ca^{2+} permeation. Representative whole-cell Li^+ current recordings from wt and *nc*DHPR myotubes in response to 200 ms depolarizations from −50 to +40 mV in the presence of 100 mM external Li^+ and either 0 (**a**), 1 µM (**b**) or 3 µM (**c**) free external Ca^{2+}. Scale bars, 50 ms (horizontal), 1 pA/pF (vertical). Plots of current-voltage relationship are depicted at the bottom of the corresponding representative Li^+ current traces. Inward Li^+ currents with no blocking ion (free $[Ca^{2+}]$=0) were indistinguishable (p>0.05) between *nc*DHPR (I_{max} = −2.32 ± 0.35 pA/pF; *n* = 16) and wt (I_{max} = −2.07 ± 0.47 pA/pF; *n* = 9) myotubes (**a**, *bottom*). However, at higher external $[Ca^{2+}]$ of 1 µM (**b**) and 3 µM (**c**), inward Li^+ currents were significantly (p<0.001) smaller in *nc*DHPR (I_{max} = −0.47 ± 0.10 pA/pF, *n* = 8; I_{max} = −0.06 ± 0.02 pA/pF; *n* = 7, respectively) compared to wt myotubes (I_{max} = −1.68 ± 0.25 pA/pF, *n* = 6; I_{max} = −0.24 ± 0.04 pA/pF; *n* = 6, respectively). (**d**) Four-parameter fitted concentration-response curves of Ca^{2+} block of inward Li^+ currents for wt and mutant *nc*DHPR. Averaged I/I_0 peak currents are plotted as a function of free external Ca^{2+} concentrations (up to 30 µM) and each data point is an average of 5–16 myotubes (***Table 1***). There is a significant (p<0.01) shift in IC_{50} (*grey dotted lines*) between wt (IC_{50} = 1.57 µM) and *nc*DHPR (IC_{50} = 0.37 µM) indicating a 4.2-fold higher Ca^{2+} pore-binding affinity in the mutant DHPR(N617D) channel. Data are presented as mean ± SEM; p determined by unpaired Student's *t*-test.

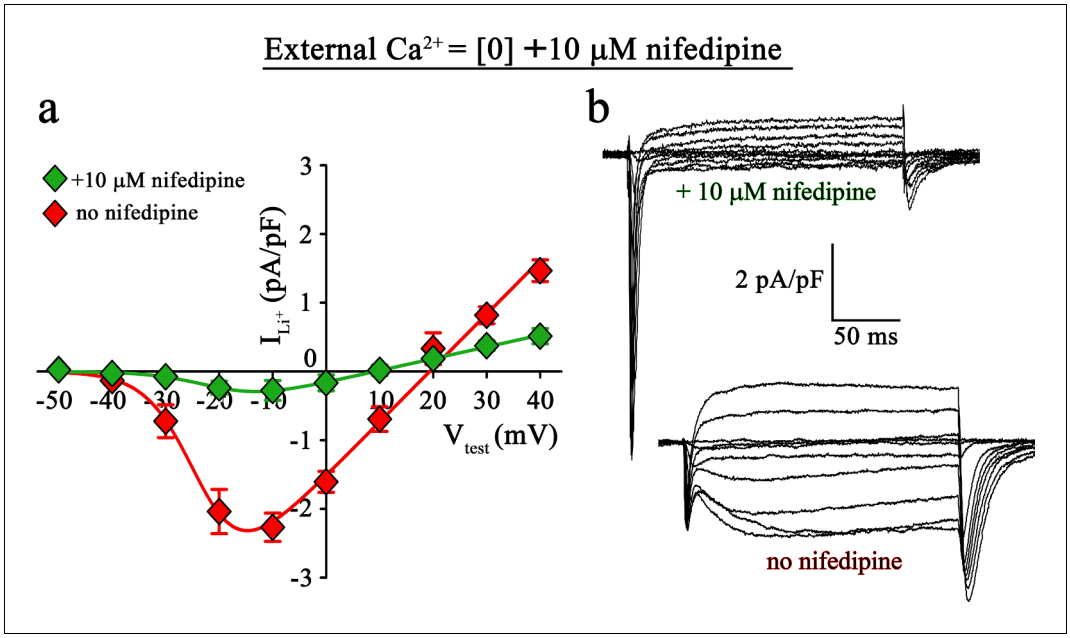

Figure 4. Inward Li^+ currents conducted by DHPR(N617D) are sensitive to nifedipine block. (**a**) Plots of current-voltage relationship for DHPR-mediated Li^+ currents recorded from *nc*DHPR myotubes in the presence (I_{max} = −0.35 ± 0.13 pA/pF; *n* = 16) and absence (I_{max} = −2.41 ± 0.27 pA/pF; *n* = 11) of 10 μM of the 1,4-DHP antagonist nifedipine, 100 mM external Li^+, and free external Ca^{2+} = [0]. Maximum inward Li^+ currents were significantly ($p<0.001$) reduced in the presence of nifedipine. (**b**) Representative whole-cell Li^+ current recordings from *nc*DHPR myotubes in response to 200 ms depolarizations from −50 to +40 mV in the presence (*upper*) and absence (*lower*) of 10 μM nifedipine with 100 mM external Li^+ and 0 external Ca^{2+} concentration. Scale bars, 50 ms (horizontal), 2 pA/pF (vertical). Data are presented as mean ± SEM; p determined by unpaired Student's *t*-test.

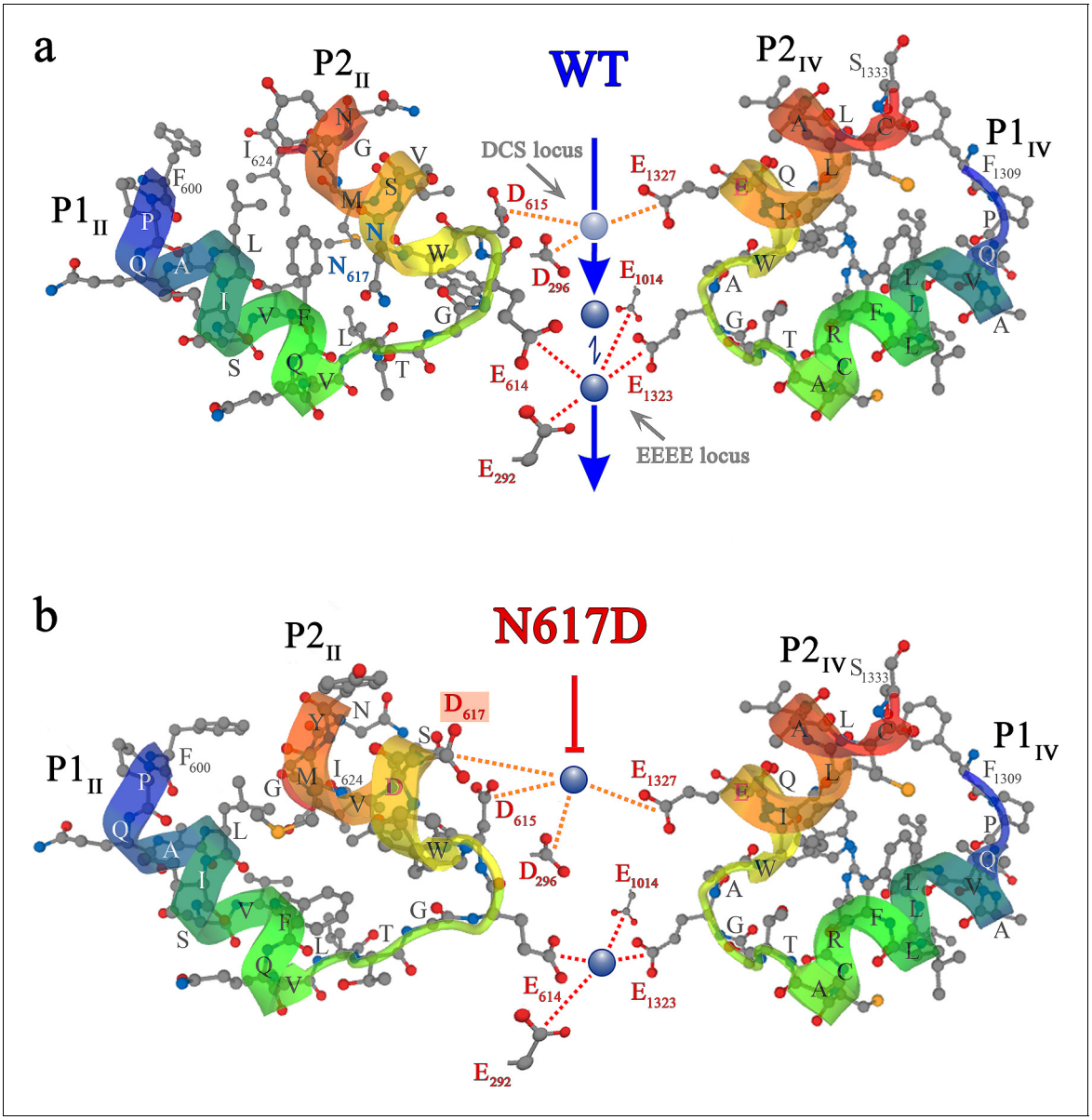

Figure 5. Ca^{2+} selectivity and conductance mechanisms in the wt and mutant DHPR(N617D) channel pore. (**a, b**) De novo conformation prediction of peptide F_{600} - I_{624} constituting the selectivity filter and adjacent pore helices P1 and P2 of DHPRα_{1S} repeat II ($P1_{II}$, $P2_{II}$) (*left*) and of peptide F_{1309} - S_{1333} forming the opposite repeat IV ($P1_{IV}$, $P2_{IV}$) (*right*), using the program PEP-FOLD 3.5 (***Thévenet et al., 2012***) on the RPBS web portal. Resulting clusters from 200 independent simulations were sorted by sOPEP energy (***Wang et al., 2011***) to yield the 'best model' prediction. Biasing the model prediction of these peptides by imposing the reference structure of DHPRα_{1S} according to the Protein Data Bank (PDB accession number 5GJV) (***Wu et al., 2016***) did not lead to major differences compared to unbiased modeling approaches and hence we used unbiased models for the wt (**a**) and DHPR(N617D) (**b**) inner channel pore. Depicted best models are graphical overlays of *cartoon* and *balls and sticks* input style options. Models depict the hypothetical mechanism of Ca^{2+} conductance through the wt DHPR (**a**) and the block of Ca^{2+} conductance due to atypical high Ca^{2+} binding affinity (because of introduction of the negative charge D_{617}; b*oxed in red*) in the DHPR(N617D) pore region. *Dotted lines* indicate binding interactions between Ca^{2+} ions (*blue spheres*) and carboxyl oxygens (*red balls*) of glutamate E_{292} and aspartate D_{296} of repeat I, E_{614}, D_{615}, and D_{617} of repeat II, E_{1014} of repeat III, as well as E_{1323} and E_{1327} of repeat IV. Low affinity Ca^{2+} binding is indicated with a *light blue sphere* and high-affinity binding with *dark blue spheres. DCS locus* is the divalent cation selectivity filter (***Cens et al., 2007***) and *EEEE locus* is the Ca^{2+} selectivity filter. Vertical *blue arrows* indicate active Ca^{2+} conductance pathway in wt DHPR (**a**) and *red T-bar* indicates block of Ca^{2+} flux by aberrant high-affinity binding to the DCS locus in the mutant DHPR (N617D) channel pore (**b**). See ***Figure 5—figure supplement 1*** for additional blocking strategies of DHPR Ca^{2+} conductance in the evolution of skeletal muscle EC coupling.

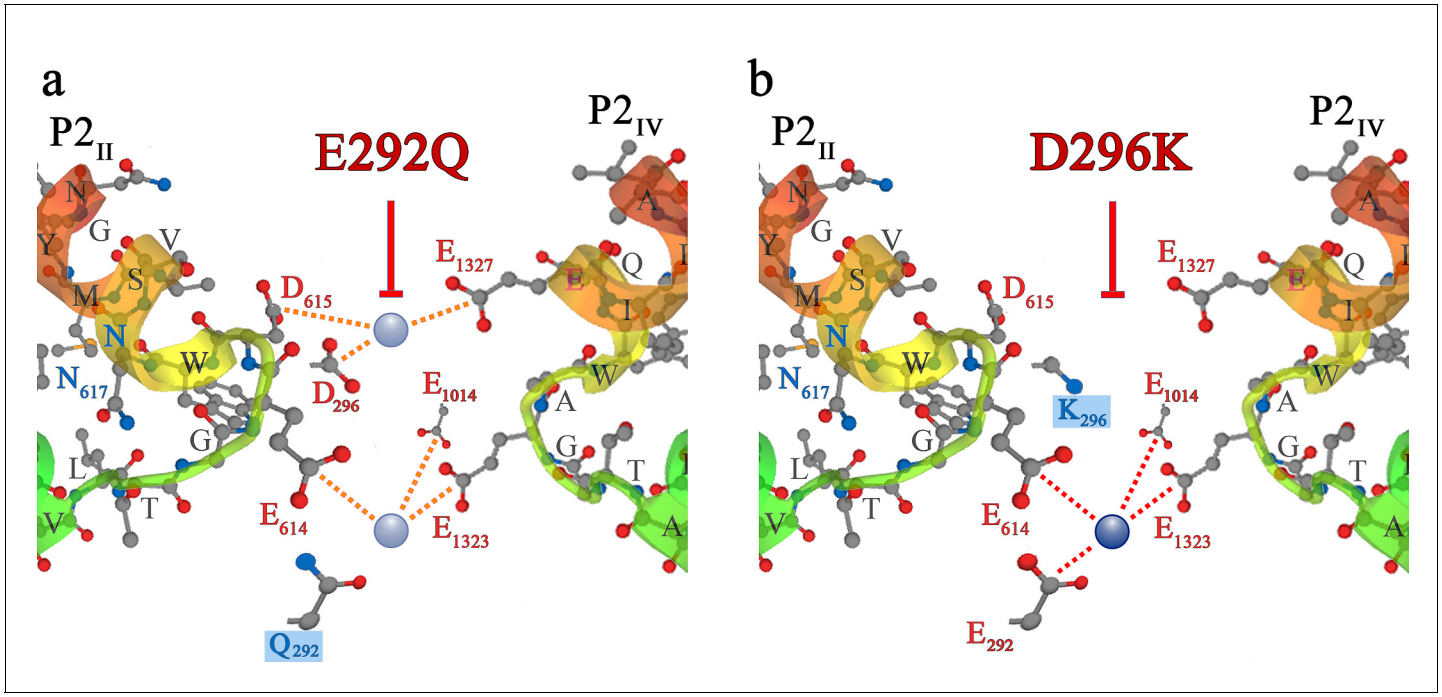

Figure 5—figure supplement 1. Additional blocking strategies of DHPR Ca^{2+}conductance in the evolution of skeletal muscle EC coupling. Symbols and nomenclature are identical to ***Figure 5***. (**a**) Zebrafish slow-muscle specific DHPRα_{1S} carries a distorted EEEE locus, due to substitution of E_{292} of repeat I by Q. Exchange of E_{292} with Q_{292} (*boxed in blue*) in rabbit DHPRα_{1S} yielded mutant DHPR(E292Q) which lacks Ca^{2+} conductance (*red T-bar*) due to alteration of the high-affinity EEEE locus to a low affinity QEEE motif. (**b**) In phylogenetically advanced teleost species, the DCS locus is distorted due to charge conversion, that is exchange of D with K in repeat I. Substitution of D_{296} with K_{296} (*boxed in blue*) in rabbit DHPRα_{1S} yielded mutant DHPR(D296K), which lacks Ca^{2+} conductance (*red T-bar*) due to non-binding of Ca^{2+} to the DCS locus and thus, lack of the attraction mechanism for t-tubular Ca^{2+}.

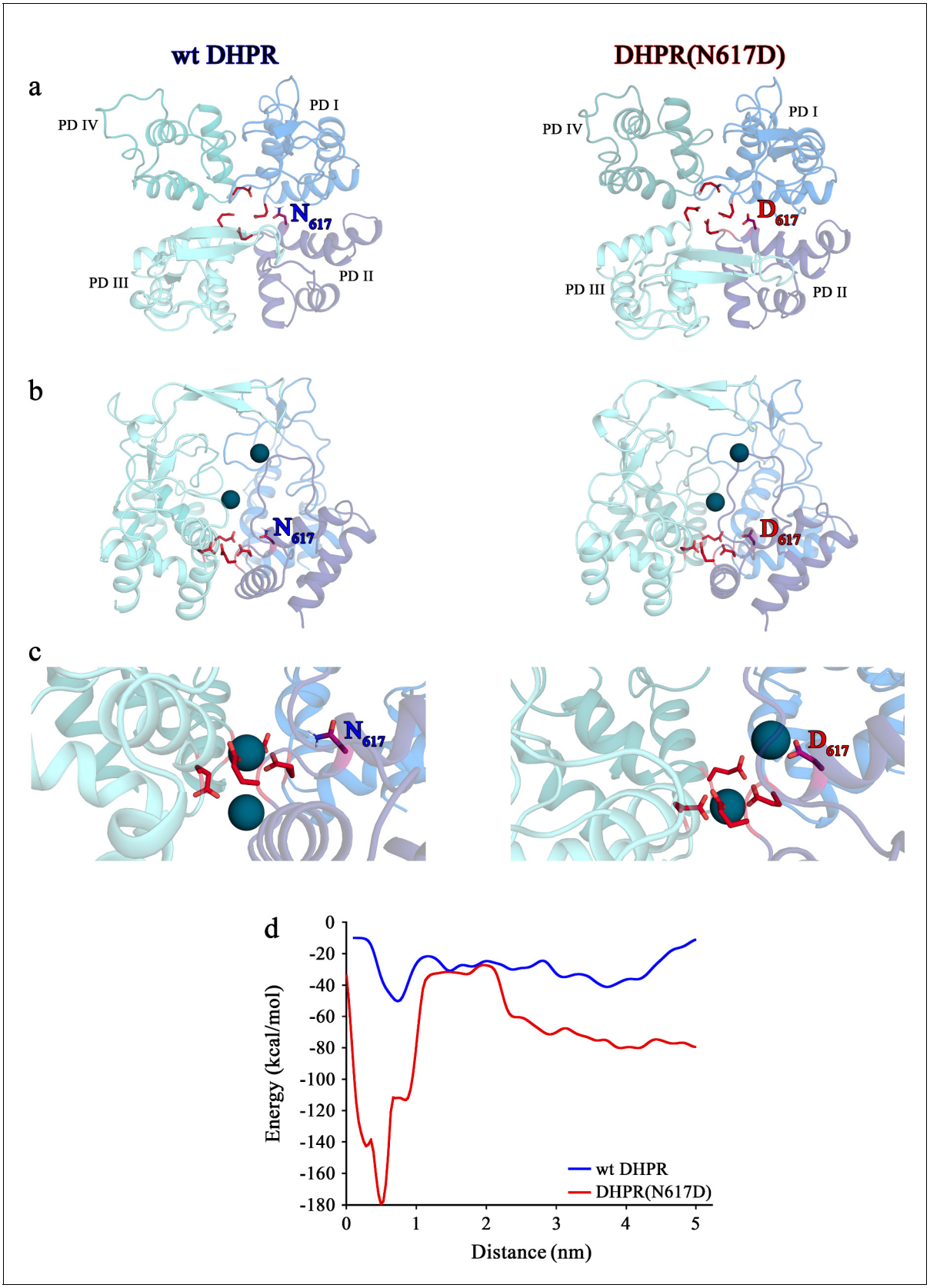

Figure 6. Structure models of selectivity filter regions of wt DHPR (*left panels*) and mutant DHPR(N617D) channel pores (*right panels*) showing the movements of Ca^{2+} ions in simulation studies. (**a**) Top view of the pore illustrating the EEEE and DCS loci. The residues of the EEEE locus are

Figure 6 continued on next page

Figure 6 continued

displayed in *red* and the DCS locus is indicated by the position of the residues N_{617} or D_{617}. (**b**) Side view of wt DHPR and mutant DHPR(N617D) pores with Ca^{2+} ions present in the pore before starting the equilibration. The *dark blue spheres* represent van der Waals radii of the Ca^{2+} ions. (**c**) Snapshots immediately following the equilibration run show that Ca^{2+} ions already moved towards the DCS and EEEE loci. While the front Ca^{2+} ion already leaves the selectivity filter of the wt DHPR toward the cytosolic side, Ca^{2+} ions in the DHPR(N617D) pore are still bound to the DCS and EEEE loci. (**d**) Free energy estimations from metadynamics simulations capturing the movements of Ca^{2+} ions through the selectivity filter region. The free energy profile for the passage of Ca^{2+} ions through wt DHPR selectivity filter is depicted in *blue* and for mutant DHPR(N617D) in *red*. The energy barrier of the Ca^{2+} ion leaving the wt DHPR selectivity filter (15 ± 4 kcal/mol; $n = 5$) is significantly smaller ($p<0.001$) compared to DHPR(N617D) (122 ± 20 kcal/mol; $n = 5$). The process was described by a one-dimensional collective variable that is, the displacement of a Ca^{2+} ion along the axis of the channel pore. A second Ca^{2+} was directly present in the simulation domain. Thus, the energy profile corresponds to the energy experienced by the first Ca^{2+} ion in the presence of the second one. See ***Figure 6—video 1*** and ***Figure 6—video 2*** for illustration of the movement of Ca^{2+} ions through the selectivity filter region of wt DHPR and DHPR(N617D) channel pores, respectively.